Penerbit Akademia Baru

Journal of Advanced Research in Fluid Mechanics and Thermal Sciences

Journal homepage: www.akademiabaru.com/arfmts.html
ISSN: 2289-7879

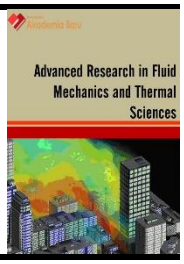

The Effect of Grooves and Permeable Plates on the Control of Vortex Shedding Behind a Single Circular Cylinder

Open Access

Zouhaier Hafsia [1,*], Saliha Nouri[1]

[1] Department of Physics, Qassim University – College of Science and Arts at Al-Rass, Saudi Arabia

ARTICLE INFO

Article history:
Received 15 September 2019
Received in revised form 8 December 2019
Accepted 10 December 2019
Available online 4 March 2020

Keywords:
Vortex shedding; passive control; shorter splitter plate; permeable plates; grooves; unconfined flow; isolated cylinder; drag reduction; fast Fourier transform (FFT)

ABSTRACT

Two permeable plates and two longitudinal grooves are proposed to control the vortex shedding behind a circular cylinder at Reynolds number $R_e = 100$. This passive control method constitutes a new alternative to reduce the drag and lift forces using a shorter splitter plate. The unsteady fluid flow is unconfined and governed by the two-dimensional Navier-Stokes equations. These governing equations are solved by the finite volume method with the higher-order QUICK scheme (Quadratic Upstream Interpolation for Convective Kinematics) for the convection fluxes. The numerical model was validated for isolated cylinder at $R_e = 20$ (steady flow) and $R_e = 100$ (unsteady flow) and well agreement was found in terms of the global and flow characteristics along the cylinder wall. The numerical results show that the periodic vortex shedding is well reproduced without introducing any physical perturbation. Compared to the isolated cylinder, the simulated results show that the vortex shedding is considerably reduced under the effect of two grooves and two permeable plates. The drag coefficient is reduced by 19% and the amplitude of fast Fourier transform (FFT) of the lift coefficient signal is considerably reduced. The porosity is taken equal to $\beta = 0.22$ and the length of the two plates is equal to one diameter of the cylinder.

1. Introduction

The periodic vortex shedding occurs due to high adverse pressure gradient imposed by the geometry of the bluff body. Then, the symmetry of the streamlines around the straight line crossing the center of the bluff body disappears. This can induce the vibration of the structures and lead to excessive drag and lift forces that can affect their integrity. The external flow around bluff bodies has a great importance in many engineering applications such as offshore oil and gas platforms, cooling systems in electronic devices, pipelines and microfluidics components and heat exchanger tubes [1].

* *Corresponding author.*
E-mail address: hafsia.zouhaier@gmail.com (Zouhaier Hafsia)

Hence, it is important to propose an efficient method to control the dynamic loading over these structures.

Periodic vortex shedding appears also around oscillating bodies and enhances both heat transfer and hydrodynamics depending on oscillating amplitude, oscillation frequency and the Reynolds number [2,3]. Mittal *et al.,* analyze the laminar flow structure in the near wake region at the initial stage of the flow induced by the harmonic oscillation of a circular cylinder [4]. It has been observed that the increase in the rate of rotation alters the formation of the first vortex. Al-Mdallel *et al.,* analyze the lock-on of vortex shedding characterized by the non-synchronized flow structure and by the irregular pattern of lift coefficient [5]. Following the numerical study of Ghozlani *et al.*, the flow around an oscillating circular cylinder and a diamond prism is simulated by considering the body fixed and oscillating the whole mass of fluid [6].

Several numerical and experimental studies concern the control of the near wake flow past a fixed circular cylinder placed in uniform cross-flow. To reduce or completely suppress the loading forces on a bluff body, active or passive methods can be used [7,8]. Due to the energy consumption, the uses of active method are limited. Such method includes oscillations of the small circular cylinders (control cylinders) mounted near the main cylinder [9].

Recently, different passive control methods have been proposed to control the vortex shedding mechanism by alteration of the boundary layer, the wake patterns, and the flow separation. These methods include the alteration of the bluff body geometry [10], or modification of the surface roughness by the implementation of grooves in the upper and the lower sides of the cylinder [11]. For turbulent flow around a circular cylinder, the experimental study conducted by Zhou *et al.,* shows that the implementation of longitudinal grooves on the cylinder surface produces a small reduction of the mean drag coefficient [12].

The effect of the attached or detached splitter plate, placed upstream or downstream the bluff body, on the suppress of the vortex shedding was extensively studied [13-15]. Experimental results show that the length, the thickness of the splitter plate and the gap between the bluff body and the plate have an important role in the alteration of the near wake fluid structure. Liu *et al.,* conducted an experimental study to investigate the effect of the splitter plate on the control of vortex shedding downstream of a circular cylinder on a confined and turbulent flow regime [16]. Following this experimental study, there is an optimal value of splitter plate length on suppression of velocity fluctuations. The confined walls stabilize the near wake flow structure and delay the vortex shedding generation. For the shorter splitter plate, the vortex shedding frequency decreased compared to the isolated cylinder case (without control device). Ozkan *et al.,* show that the implementation of permeable plates along the entire span of the cylinder and normal to the surface suppresses vortex shedding by reducing the velocity fluctuations in the wake, elongating the vortex formation region further downstream and attenuating the vortex shedding frequency [17].

The main purpose of this study is to propose a passive control method permitting to suppress vortex shedding behind a circular cylinder at rest placed in uniform cross-flow. In the first stage, the laminar flow past a circular cylinder is validated based on flow variables on the cylinder surface and the drag and lift coefficients. In the second stage, the combined effects of two grooves and two permeable plates (or control plates) on the reduction of the drag force over a circular cylinder are analyzed. This proposed passive control method constitutes an alternative to one longer splitter plate.

2. Problem Configuration and Model Validations

2.1 Governing Equations and Numerical Methods

For an incompressible fluid and laminar flow, the unsteady and two-dimensional Navier-Stokes equations can be written in Cartesian coordinates in the following form

* Mass conservation equation

$$\frac{\partial u}{\partial x}+\frac{\partial v}{\partial y}=0 \tag{1}$$

* Momentum equation in x direction

$$\frac{\partial u}{\partial t}+u\frac{\partial u}{\partial x}+v\frac{\partial u}{\partial y}=-\frac{1}{\rho}\frac{\partial p}{\partial x}+\nu\left(\frac{\partial^2 u}{\partial x^2}+\frac{\partial^2 u}{\partial y^2}\right) \tag{2}$$

* Momentum equation in y direction

$$\frac{\partial v}{\partial t}+u\frac{\partial v}{\partial x}+v\frac{\partial v}{\partial y}=-\frac{1}{\rho}\frac{\partial p}{\partial y}+\nu\left(\frac{\partial^2 v}{\partial x^2}+\frac{\partial^2 v}{\partial y^2}\right) \tag{3}$$

where (x, y) are Cartesian coordinates, u and v are the velocity components respectively in x and y directions; ν is the kinematic viscosity of the water and ρ is the fluid density; p and t are respectively the pressure and time. These transport equations can be written in the following general form

$$\frac{\partial}{\partial t}(\rho\phi)+\frac{\partial}{\partial x_i}(\rho u_i\phi)=-\frac{\partial p}{\partial x_i}+\frac{\partial}{\partial x_i}\left(\mu\frac{\partial \phi}{\partial x_i}\right) \tag{4}$$

where ϕ is a transport variable corresponding to $\phi=1$ for the mass conservation equation and $\phi=u$ or v for the momentum equations; μ is the dynamic viscosity of the water. These non-linear transport equations are discretized in space using the finite volume method (FV). The convective fluxes are discretized using the QUICK higher-order scheme for computing the ϕ variable *at* the cell face from the cell centers values. This convection scheme was first used by Franke *et al.,* to investigate laminar vortex shedding past a circular cylinder [18]. Preliminary numerical tests show that the first-order upwind convection scheme lead to symmetric flow around the cylinder over each time step and this scheme is not suitable for vortex shedding flow. The time discretization is based on the implicit Euler scheme where the transport variable ϕ is determined in terms of unknown variables. It is unconditionally stable, but only a first-order accurate. The velocity-pressure coupling is solved based on the Pressure Implicit with Splitting of Operators (PISO) algorithm [19]. This algorithm was developed originally for non-iterative computation of unsteady compressible flow. It was adapted successfully for the iterative solution of steady flow. It involves one predictor step and two corrector steps. The computational domain is discretized in a Cartesian grid and a cut-cell method is used to represent the circular cylinder. This method permits to discretize more complex mesh by truncating the Cartesian grid at the boundary surface of the cylinder. The boundary variables are determined by solutions interpolation procedure.

2.2 Computational Domain

The main difficulties to accurately simulate the vortex shedding past a circular cylinder is the selection of a computational domain and the specification of outlet boundary condition to approximate the external flow having an infinite domain. Qu *et al.,* used a grid of O-type and a convective outlet boundary is fixed at $40\ D$ for R_e up to 200 where R_e is the Reynolds number based on the cylinder diameter D and the free stream velocity U∞ given by: $R_e = \frac{U_\infty D}{\nu}$ [20]. A C-grid system is used by Park *et al.,* and a convective outlet boundary is fixed at $50\ D$ for R_e up to 160 [21]. In the present study, numerical tests show that the suitable computational domain size is the same as chosen by Tawekal [22]. The shape and size of the domain are illustrated in Figure 1.

The circular cylinder with diameter $D = 0.5\ m$ is placed in the middle part of the considered computational domain in y-direction. To reduce the effect of the inflow and outflow boundaries conditions on the flow field, numerical tests show that the length of the domain from the cylinder center to inlet and outlet L_u and L_d have the following values: $L_u = 16\ D$ and $L_d = 40\ D$. The width of the computational domain W is taken equal to L_d. Following these values, the blockage ratio defined by $B_R = \frac{D}{W} = 0.025$. The same domain size is adopted for $R_e = 20$ and $R_e = 100$.

To alter the vortex shedding, the main passive control methods tested in the present study are shown in Figure 2: two permeable plates attached to the base of the cylinder denoted PP2 (Figure 2(a)), two square grooves placed on the upper and lower side of the cylinder denoted G2 (Figure 2(b)) and the non- permeable and single splitter plate (standard splitter plate): standard splitter plate denoted IP (Figure 2(c)). The combined effect of permeable plates and grooves are also considered (Figure 2(d)).

The grooves act as surface roughness and splitter plate as an extension of the cylinder geometry. In all tested cases, the length of the splitter plate is equal to $1.0\ D$ (in the limit of shorter plate) and its thickness was equal to $0.065\ D$. The location of the permeable splitter plates is defined by the attachment angle θ_f defined between the straight line crossing the attachment point and the center of the cylinder and the wake centerline (Figure 2(a)).

The entire grid of the computational domain and the cut-cell grid in the case of an isolated cylinder are shown in Figure 3. The grid is more refined close to the cylinder surface to well reproduce the flow characteristics. However, the grid density is reduced in the region away from the wake.

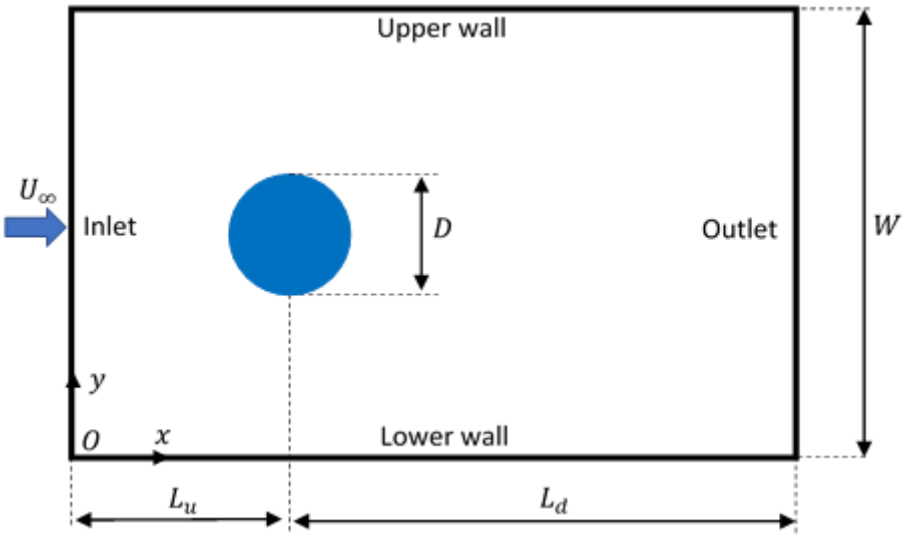

Fig. 1. Physical model and coordinate system of flow past a circular cylinder

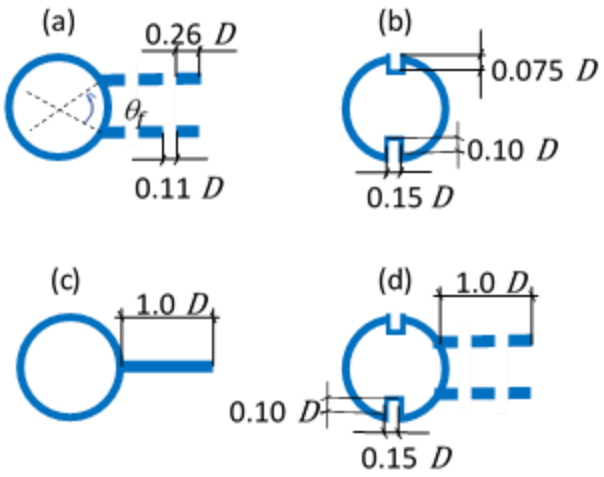

Fig. 2. Circular cylinder with the main passive control methods considered in the present study: a) two permeable plates (2PP-15), b) two longitudinal grooves (G2), c) single splitter plate and d) G2+2PP-15

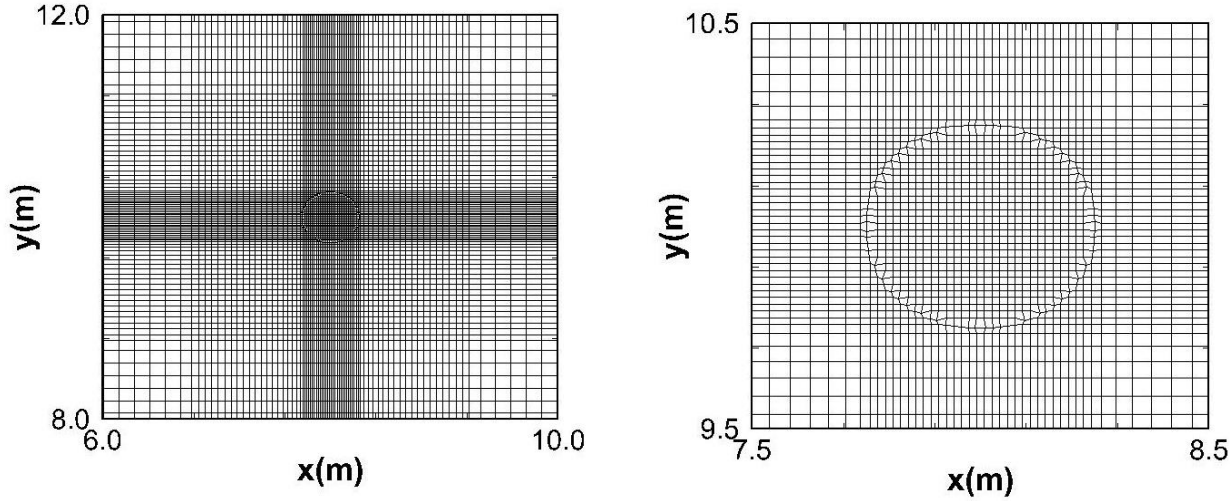

(a) (b)

Fig. 3. Grid of computational domain (a) Grid distribution around the circular cylinder (b) Cut-cell grid of the cylinder boundary

2.3 Initial and Boundaries Conditions

In the present study, all numerical simulations started using quiescent initial conditions ($u(x, y, t = 0) = v(x, y, t = 0) = 0$) which means that no physical perturbation was introduced to initiate the vortex shedding formation. The vortex shedding outcome of the numerical solutions triggered by round-off errors. The vortex shedding can be initiated by physical perturbation imposed numerically for a short time such as a clockwise rotation of the circular cylinder followed by counter-clockwise rotation [23]. The following boundaries conditions are considered

* At the domain inlet, a uniform free stream velocity is prescribed: $u(x = 0, y, t) = U_\infty$ and $v(x = 0, y, t) = 0$. The considered Reynolds number ($R_e = 20$ and $R_e = 100$) are obtained by fixing

the inlet velocity $U_\infty = 1\ m/s$. In order to avoid a very long transit time of simulation, the desired R_e are obtained by modifying the kinematic viscosity instead of U_∞.

* At the cylinder surface described by the coordinates (x_c, y_c) and at the top and bottom walls, no slip condition were applied

$$u(x_c, y_c, t) = 0, v(x_c, y_c, t) = 0 \text{ and } u(x, y = 0, t) = 0, v(x, y = W, t) = 0 \quad (5)$$

* At the outlet boundary the pressure is prescribed equally to zero: $p(x = L_u + L_d, y) = 0$ and the normal derivative of the tangential velocity is set to zero $\left(\frac{\partial v}{\partial x}\right)_{outlet} = 0$

Inflow and outflow boundary conditions are placed far from the circular cylinder to reduce any undesired interaction with the main flow region, especially between the outlet and the flow at the rear end of the cylinder.

3. Validation of the Proposed Model

3.1 Validation Procedure

The steady and unsteady flow past a circular cylinder is extensively studied but a few investigations contain details about the flow field on the cylinder surface. First, the steady flow behind a circular cylinder for $R_e = 20$ is presented in order to validate the cut-cell approach of the present numerical model. Then, the periodic vortex shedding for $R_e = 100$ is validated for an isolated cylinder. In this study, the global flow characteristics and also the flow field variables on the cylinder surface are compared with previous numerical or experimental results. The distributions of the pressure coefficient C_P and the spanwise vorticity Ω along the cylinder surface and the distribution of streamwise velocity u along the wake centerline were presented and analyzed.

For unsteady flow field past a circular cylinder, a global validation based on time-averaged drag coefficient $< C_D >$, time-averaged lift coefficient $< C_L >$ and Strouhal number S_t are presented. The $< C_D >$ expresses the ratio of the time-averaged drag force $< F_D(t) >$ to the dynamic pressure times the area ($A = D * 1$) and given by

$$< C_D >= \frac{< F_D(t) >}{0.5\ \rho\ U_\infty^2\ D} \quad (6)$$

Using, the time-averaged lift force $< F_L(t) >$, the $< C_D >$ can be defined by:

$$< C_L >= \frac{< F_L(t) >}{0.5\ \rho\ U_\infty^2\ D} \quad (7)$$

Based on the fast Fourier transform (FFT) of C_L signal, the frequency of the vortex shedding f_s can be determined. This frequency permits the calculation of the Strouhal number by the following relation

$$S_t = \frac{f_s\ D}{U_\infty} \quad (8)$$

The drag and lift coefficients and Strouhal number are dimensionless.

The flow field variables on the cylinder surface concern the distributions of time-average pressure coefficient $< C_P >$ and mean spanwise vorticity $< \Omega >$ along the cylinder wall and mean streamwise velocity distribution along the wake centerline. The $< C_P >$ is defined as

$$< C_P >= \frac{<p>-p_\infty}{0.5\,\rho\,U_\infty^2} \tag{9}$$

where $< p >$ and p_∞ are respectively the mean pressure and the reference pressure determined at the inlet section which is depended on the domain dimension.

From the time-average velocity field, the spanwise vorticity component is determined by:

$$< \Omega >= \frac{\partial <v>}{\partial x} - \frac{\partial <u>}{\partial y} \tag{10}$$

where $< u >$ and $< v >$ are the time-average velocity components respectively in x and y directions.

3.2 Validation for Steady Flow at $\boldsymbol{R_e = 20}$

For this Reynolds number, the flow is steady and the cut-cell method can be easily validated. Also, the flow patterns past a circular cylinder at this Reynolds number is well documented which justify the choice of this flow configuration for validation. The present numerical results are compared with the available experimental results at the same Reynolds number reported by Tritton [24] and computed results conducted by Nieuwstadt *et al.,* [25].

The computed drag coefficient $C_D = 2.12$ is very close to the experimental value equal to $C_{D,exp} = 2.05$. As shown in Figure 4, the simulated streamlines are symmetrical around the centerline of the cylinder and presented two attached vortices with two focal points.

The point where the velocity of the wake is equal to zero is known as the wake stagnation point S_W. The distance between the cylinder base and wake stagnation point is known as recirculation length L_R. The present study shows that $L_R = 0.93\ D$ which compares well with experimental results. The separation point in the boundary layer of the circumference of the cylinder corresponds to the point where the wall vorticity is zero. The corresponding separation angle from the rear stagnation point occurred at $\theta_s = 41.0^o$ which is around the experimental value $\theta_{s,exp} = 41.6^o$. The higher pressure coefficient corresponding to the front of the stagnation point agrees very well with the computed results of Nieuwstadt *et al.,* [25]. However, the minimum value of C_P separating the accelerating and decelerating regions is slightly different from the previously computed results. The minimum fluid velocity in the wake occurs at position $0.42\ D$ away from the cylinder base and the minimum velocity in the wake is $-0.03\ U_\infty$. These results agree very well with the previous experimental results of Tritton [24].

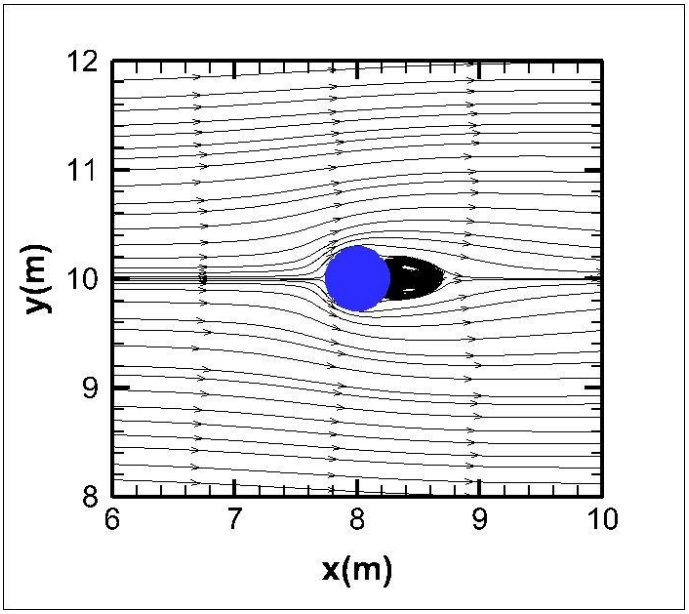

Fig. 4. Streamlines for steady and laminar flow past a circular cylinder at $R_e = 20$

3.3 Validation for Unsteady Flow Characteristics at $\boldsymbol{R_e = 100}$

The isolated cylinder denoted a circular cylinder without a control device, constitutes a reference case for comparison with the simulated results of a circular cylinder with control devices. The grid and time-step independence for an isolated cylinder were conducted by comparison of the present numerical results with the previous numerical results of Qu *et al.,* [20]. Denoting Nx and Ny the grid numbers along x and y directions respectively, three grids have been tested

* Grid1 (a fine grid): $Nx_1 * Ny_1 = 260 * 210$
* Grid2 (a medium grid): $Nx_2 * Ny_2 = 240 * 182$
* Grid3 (a coarse grid): $Nx_3 * Ny_3 = 220 * 170$

In all tested grids, the cell size around the cylinder is $D/20$. There is no significant difference in the results produced by the Grid$_2$ and Grid$_3$. The fine grid Grid$_1$ was adopted after a complete validation of flow characteristics along the cylinder surface. The next step is to investigate the time step independence. Three time steps were tested: $\Delta t_1 = 0.020\ s$; $\Delta t_2 = 0.025\ s$ and $\Delta t_3 = 0.030\ s$. Numerical results show that time step $\Delta t_1 = 0.020\ s$ is more convenient (Figure 5). This corresponds approximately to 75 time steps per vortex shedding period.

After the grid and time step independence tests, a complete comparison of the present numerical method base on the cut-cell method is presented in Table 1.

In the present study, the mean value of C_D is equal to $< C_D >= 1.37$ (Figure 6) which close to the numerical value found by Hwang *et al.,* equal to 1.34 [30]. This computed mean value is taken after the vortex shedding formation with a fixed C_L amplitude of fluctuation for a time equal to several vortex shedding periods.

Figure 7 reported the time variation of the lift coefficient. Following this figure, the period of C_L is twice the vortex shedding period. The amplitude of C_L fluctuation is ± 0.286. This is very close to the previously computed value reported by Park *et al.,* [21].

Table 1
Comparison of flow characteristics with previous numerical and experimental studies for $R_e = 100$

Reference	$< C_D >$	$< C_L >$ amplitude	S_t
[26]	1.369	-	0.162
[27]	1.322	0.226	0.164
[28]	1.431	0.226	0.165
[21]	1.330	0.235	0.165
[29]	1.336	-	0.164
Present study	1.369	0.286	0.164

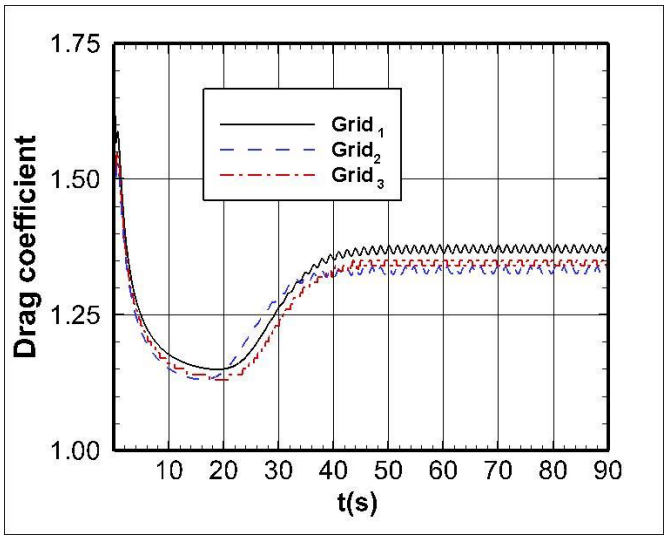

Fig. 5. Grid independence for time variation of the drag coefficient for the isolated cylinder at $R_e = 100$

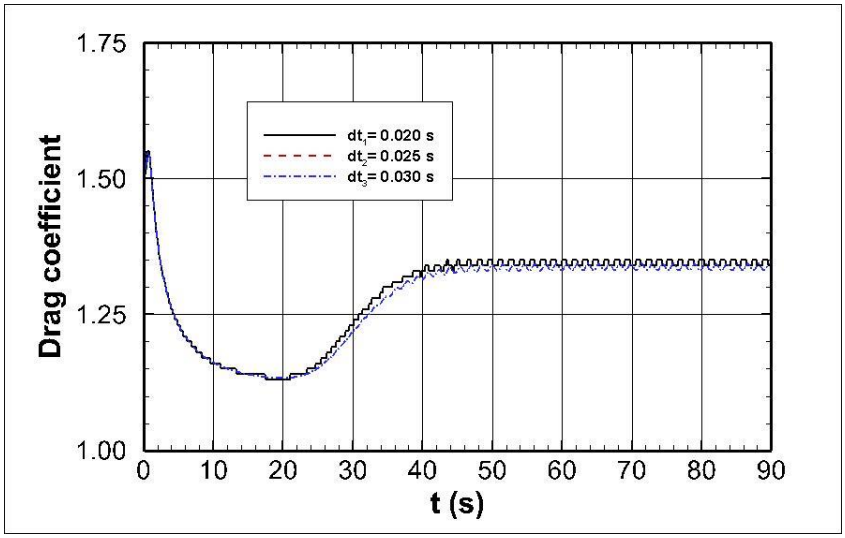

Fig. 6. Time step independence for time variation of the drag coefficient for the isolated cylinder at $R_e = 100$

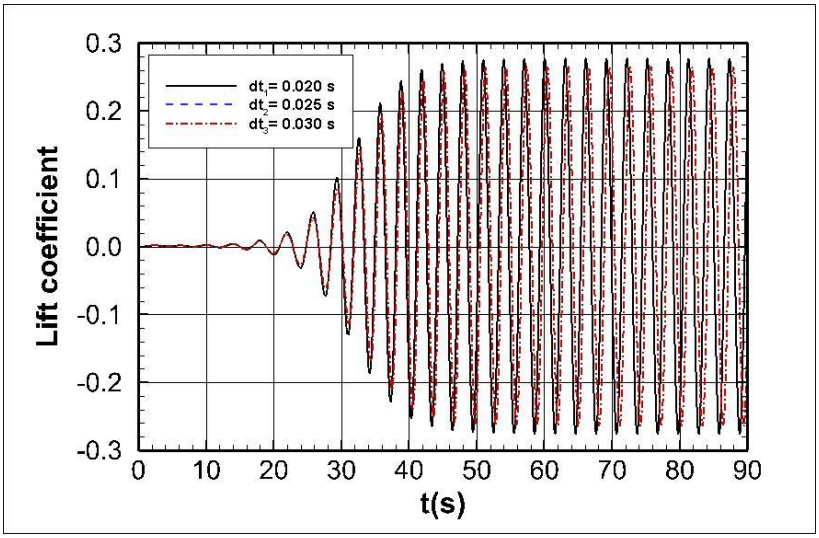

Fig. 7. Time step independence for time variation of the lift coefficient for the isolated cylinder at $R_e = 100$

The periodic character of C_L is more obvious than the drag coefficient. Hence, the C_L signal is used to quantify periodicity and the strength of the vortex shedding. It should be noted that the vortex shedding frequency f_s can be obtained from velocity and pressure time histories which oscillate within the same frequency as C_L. In the present study, the frequency fs is determined based on the fast Fourier transform (FFT) of C_L signal as illustrated in Figure 8 for grid$_1$ and Δt_1.

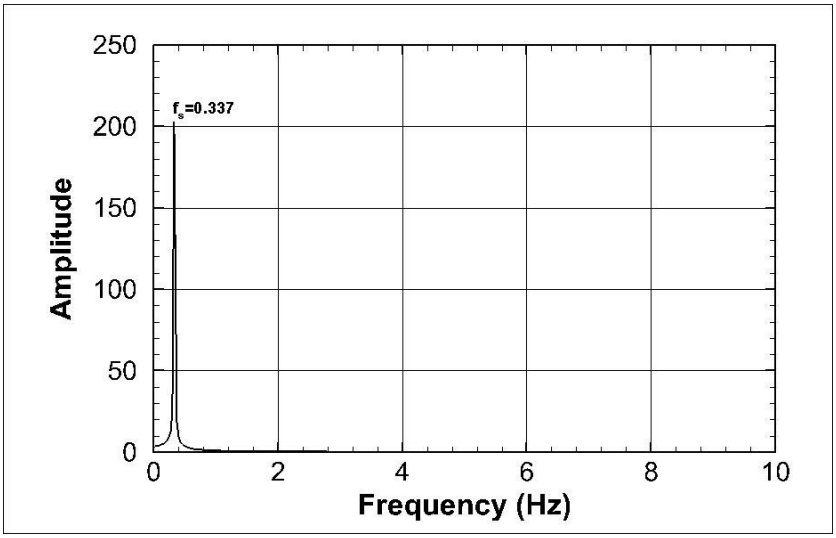

Fig. 8. Fourier spectrum for isolated cylinder at $R_e = 100$

For an isolated cylinder and due to the periodic nature of vortex shedding, a dominant peak was observed at $f_s = 0.328\ Hz$. The corresponding Strouhal $S_t = 0.164$ for $R_e = 100$. According to the numerical study of Hwang *et al.,* [30], the Strouhal number is 0.167. This small discrepancy between these two results can be attributed to the discrepancy in the computation of the unsteady separation angles in the upper and lower sides of the cylinder.

The distributions of the pressure coefficient C_P and the spanwise vorticity Ω_{ad} along the cylinder surface and the distribution of streamwise velocity u along the wake centerline were presented respectively in Figure 9, 10 and 11. A comparison with computed results of Qu *et al.,* is found to be satisfactory [20].

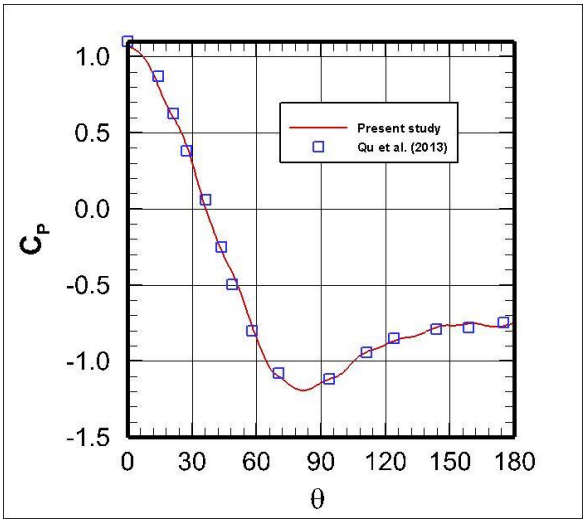

Fig. 9. Pressure coefficient on the cylinder surface at $R_e = 100$

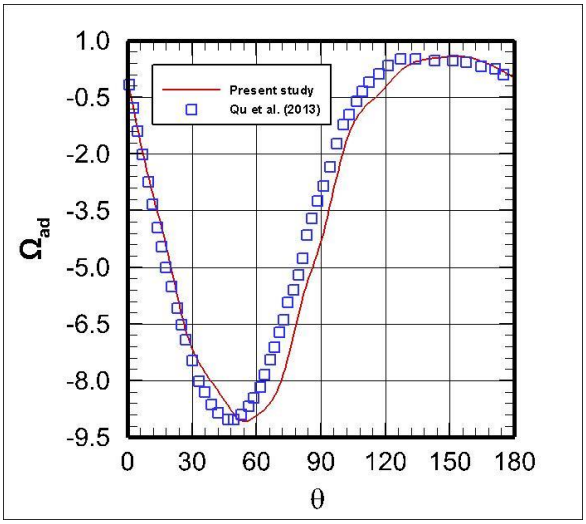

Fig. 10. Spanwise vorticity on the cylinder surface at $R_e = 100$

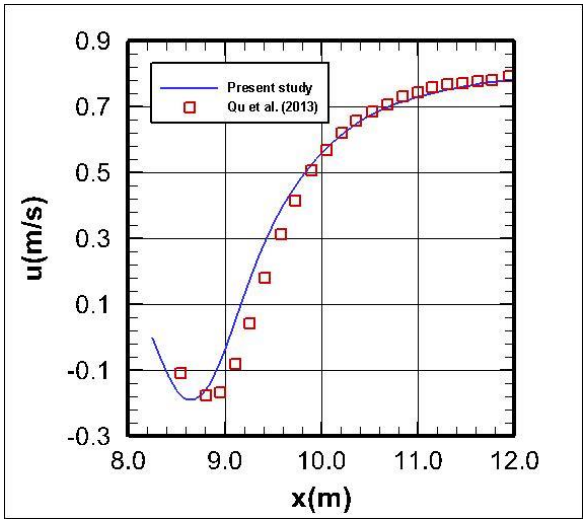

Fig. 11. Rear streamwise velocity for steady flow past a circular cylinder at $R_e = 100$

In Figure 12, instantaneous streamlines in the near wake region are plotted at four instants over a single period of vortex shedding $T = 1/f_s$. Instant A ($t = t_0 = 47.95\ s$), corresponds to the peak of C_L. At this instant, a large clockwise vortex is detaching from the upper surface of the cylinder. This detached vortex moves toward the viscous wake (Figure 12(a)). At instant B ($t = t_0 + T/4$), (the first zero value of C_L), the anticlockwise structure detaches from the lower cylinder surface and is incorporated into the viscous wake (Figure 12(b)). Figure 12(c) shows the instantaneous streamlines at instant C ($t = t_0 + T/2$), (lowest value of C_L). From Figure 12(c) and 12(a), the separated vortex alternately shed from upper and lower sides of the cylinder with the defined frequency f_s and the vortex shedding is well simulated. Figure 12(d) shows the instantaneous streamlines at instant D ($t = t_0 + 3T/4$), (the last zero value of C_L). From Figure 12(d) and 12(b), the vortex is also shed symmetrically.

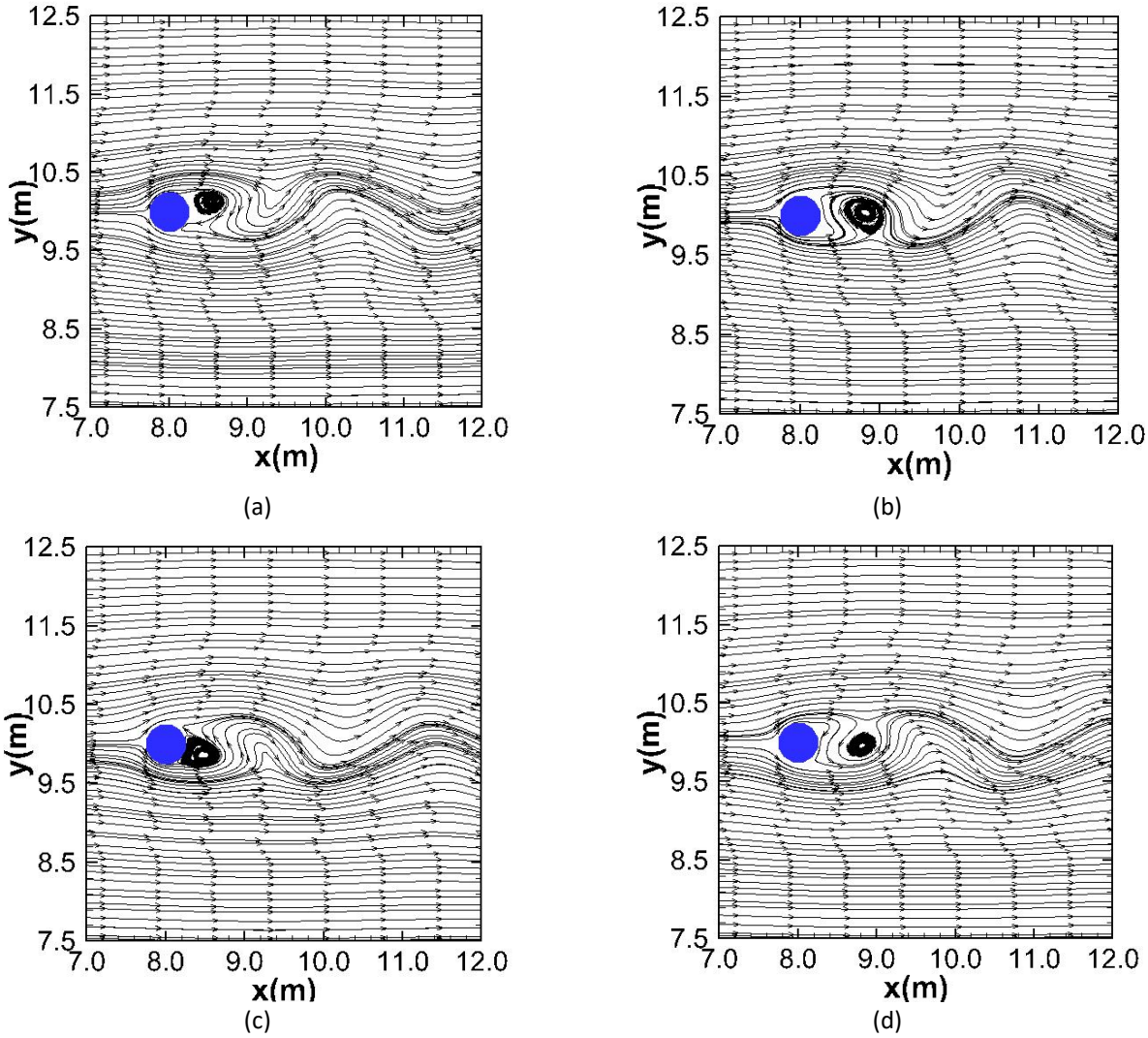

Fig. 12. Instantaneous streamlines for the isolated cylinder at $R_e = 100$: a) $t = t_0$, b) $t = t_0 + T/4$, c) $t = t_0 + T/2$ and d) $t = t_0 + 3T/4$

4. Effect of the Control Plates and Grooves

The effect of the proposed passive control device are analyzed in terms of mean streamlines patterns, mean spanwise vorticity, the vortex shedding frequency, the variation of the C_L amplitude and the mean drag reduction compared to the isolated cylinder. To suppress the vortex shedding,

two grooves with a pair of permeable plates were implemented and denoted (G2+PP2). These grooves are located in the upper and lower cylinder surface and having the dimension illustrated in Figure 2. Different numerical simulations were undertaken by varying the porosity factor β and the attachment angle θ_f relative to free stream direction. A comparison between numerical results shows that the suppression of vortex shedding is obtained with two permeable plates with porosity $\beta = 0.22$ and attachment angle $\theta_f = 15^o$ relative to free stream direction.

In all tested cases, the control plates are attached to the rear of the cylinder and plate length L is maintained equal to $1D$ in order to determine the efficiency of a short and permeable plate in terms of vortex shedding suppression. However, in the previous numerical or experimental studies, the length L is varied, from $1D$ to $5D$, to determine the optimal value of L that suppress the vortex shedding.

4.1 Time-Averaged Flow Patterns

The computed results for permeable plates and longitudinal grooves are compared to the isolated cylinder results at $R_e = 100$. Figure 13 illustrated the mean streamlines and the mean spanwise vorticity behind the circular cylinder with and without control devices implementation. Compared to the isolated cylinder (Figure 13(a)), the two up and low grooves do not induce a significant difference in the flow structure in terms of recirculation length but the magnitude of vorticity is changed (Figure 13(b)). Furthermore, the mean streamlines and spanwise vorticity remains quasi-symmetric with respect to cylinder centerline (Figure 13(a) and 13(b)). The permeable splitter plate reduces the vortex shedding near the circular cylinder by reducing the interaction between the two separated free shear layers (Figure 13(c)).

The standard splitter plate elongates the recirculation region and the flow becomes unsteady further downstream causing the shedding to be weaker (Figure 13(d)). The recirculation length for two permeable splitter plates and two longitudinal grooves is longer than for isolated cylinder (Figure 13(a) and 13(e)). In addition, the amplitude of mean spanwise vorticity is the same as the isolated cylinder.

4.2 Drag and Lift Coefficients

The suppression of vortex shedding can be analyzed in terms of the variation of C_D and C_L with time. Figure 14 presents the time evolution of the drag coefficient for two types of control devices: two grooves (G2) and two permeable plates at angle 15° combined to two grooves (G2+PP2-15). The time evolution of C_D is compared to the isolated cylinder. For (G2), the $< C_D >= 1.31$ is significantly lower than that of the isolated cylinder $< C_D >= 1.37$ (4.4 % lower). Under the effect of (G2), the vortex shedding period is equal $1.50\ s$ which is almost equal to the period of the isolated cylinder.

The combined grooves and plates reduce the $< C_D >$ to 1.12 and the reduction ratio is 19 %. The time variations of C_L for the grooves and permeable plates compared to the isolated cylinder are illustrated in Figure 15. In all simulated cases, the lift force fluctuates at a regular frequency and the maximum amplitudes of C_L are only around $\pm$ 0.074 for the proposed control devices (G2+PP2-15). These amplitudes are around $\pm$ 0.25 for two grooves without plates.

Figure 16 reports the power spectrum of the lift coefficient. The FFT curve has a single sharp peak at a predominant frequency for isolated cylinder and the amplitude is considerably reduced in the case of the proposed solution (G2+PP2-15). Hence, by the implementation of this control device, the vortex shedding is suppressed.

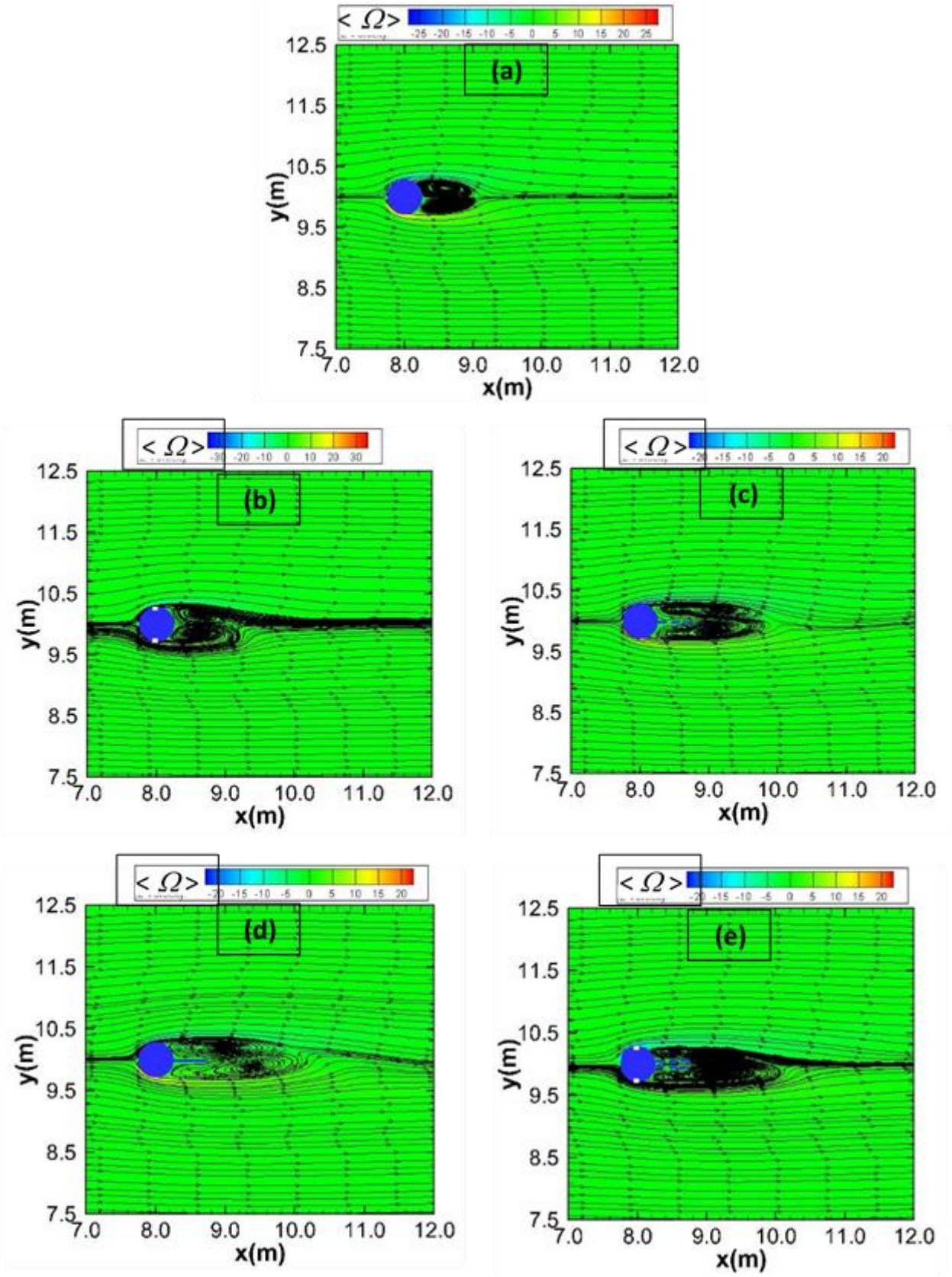

Fig. 13. Mean streamlines and spanwise vorticity contours at $R_e = 100$: a) Isolated cylinder; b) G2; c) Attached PP; d) Attached splitter; G2+PP-15

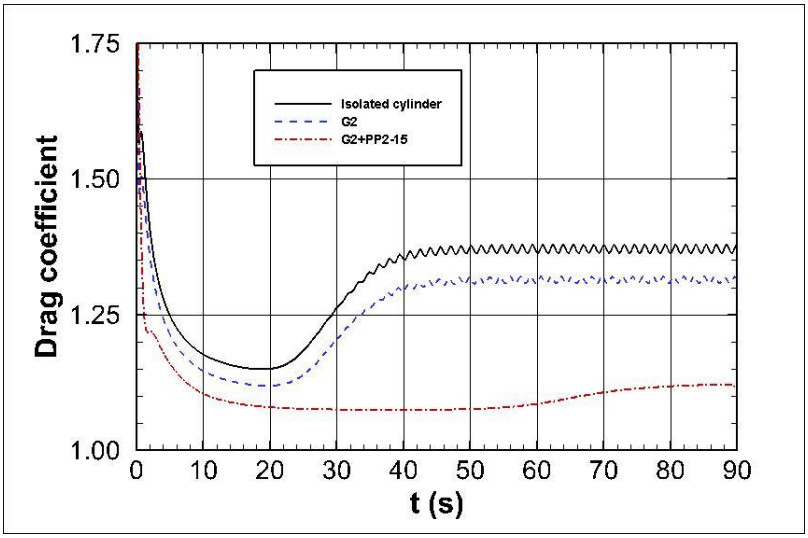

Fig. 14. Comparison between the time variation of the drag coefficient with and without control devices at $R_e = 100$

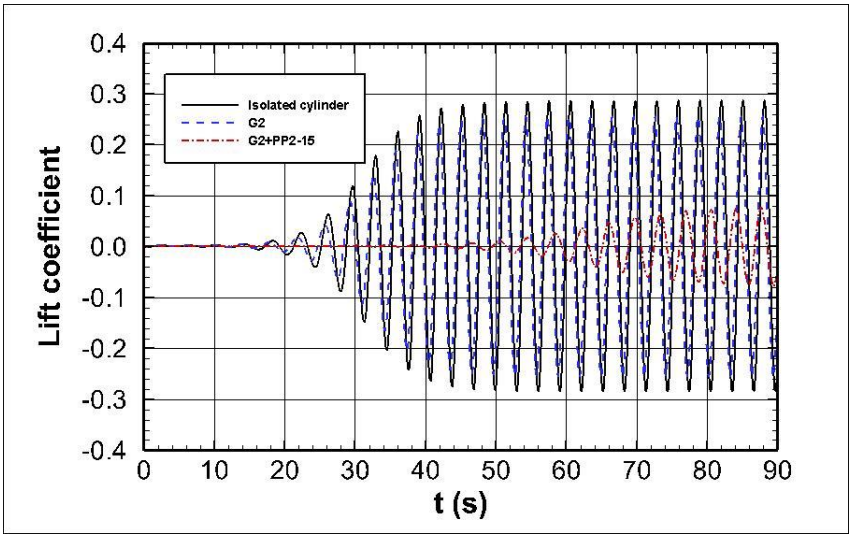

Fig. 15. Comparison between the time variation of the lift coefficient with and without control devices at $R_e = 100$

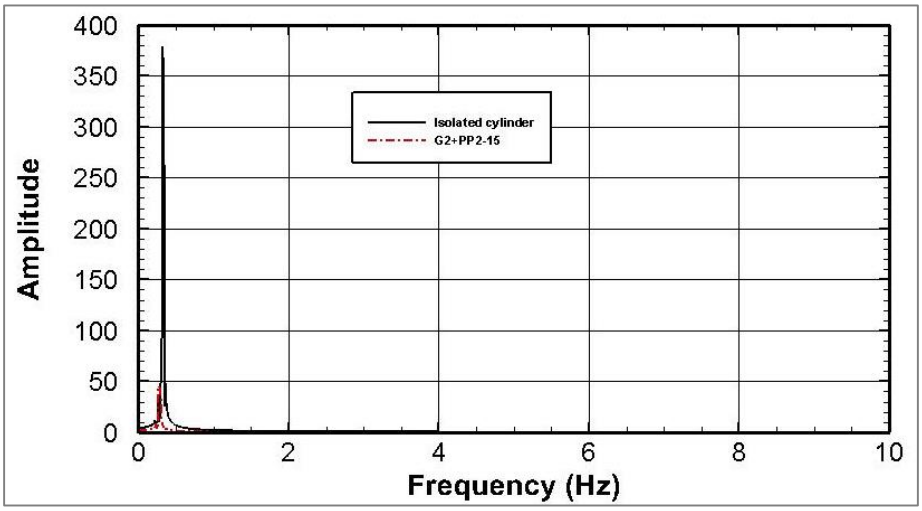

Fig. 16. Fourier spectrum for the isolated cylinder and two grooves combined to two permeable plates at $R_e = 100$

5. Conclusions

The flow structure behind a circular cylinder is analyzed for two laminar flow regimes $R_e = 20$ (steady flow) and $R_e = 100$ (unsteady flow). The validation procedure was conducted in terms of global and cylinder wall flow characteristics. For steady flow at $R_e = 20$, numerical results show a good agreement with the available experimental study in the main flow features including the separation angle, drag coefficient, and recirculation length. For $R_e = 100$, the flow becomes unsteady and the periodic vortex shedding from the upper and lower cylinder surface is well reproduced.

Numerical results show that the number of permeable plates and their positions considerably affects the near wake flow. The maximum reduction of C_D equal to 19% is obtained with two permeable splitter plates attached to the rear base point of the cylinder at an attachment angle of 15^o combined with two longitudinal grooves for the considered $R_e = 100$. As an extension of this study, we can investigate the flow interference induced by multiple bluff bodies: tandem, side-by-side or staggered arrangements. The positions and types of vortex shedding control for different gap spacing will be tested by the proposed model based on the immersed boundary to reproduce a more complex body shape.

Acknowledgements
The authors gratefully acknowledge Quassim University, represented by the Deanship of Scientific Research, on the material support for this research under the number 3572-alrasscac-2018-1-14-S during the academic year 1437 AH/2016 AD.

References

[1] Chauhan, Manish Kumar, Sushanta Dutta, Bhupendra Singh More, and Bhupendra Kumar Gandhi. "Experimental investigation of flow over a square cylinder with an attached splitter plate at intermediate Reynolds number." *Journal of Fluids and Structures* 76 (2018): 319-335.
[2] Mittal, H. V. R., and Qasem M. Al-Mdallal. "A numerical study of forced convection from an isothermal cylinder performing rotational oscillations in a uniform stream." *International Journal of Heat and Mass Transfer* 127 (2018): 357-374.
[3] Al-Mdallal, Q. M., and F. M. Mahfouz. "Heat transfer from a heated non-rotating cylinder performing circular motion in a uniform stream." *International Journal of Heat and Mass Transfer* 112 (2017): 147-157.
[4] Mittal, H. V. R., Rajendra K. Ray, and Qasem M. Al-Mdallal. "A numerical study of initial flow past an impulsively started rotationally oscillating circular cylinder using a transformation-free HOC scheme." *Physics of Fluids* 29, no. 9 (2017): 093603.
[5] Al-Mdallal, Qasem M., and Serpil Kocabiyik. "Rotational oscillations of a cylinder in cross-flow." *International Journal of Computational Fluid Dynamics* 20, no. 5 (2006): 293-299.
[6] Ghozlani, Belgacem, Zouhaier Hafsia, and Khlifa Maalel. "Numerical study of flow around an oscillating diamond prism and circular cylinder at low Keulegan-Carpenter number." *Journal of Hydrodynamics* 24, no. 5 (2012): 767-775.
[7] Sen, Uddalok, Achintya Mukhopadhyay, and Swarnendu Sen. "Effects of fluid injection on dynamics of flow past a circular cylinder." *European Journal of Mechanics-B/Fluids* 61 (2017): 187-199.
[8] Turki, Saïd. "Numerical simulation of passive control on vortex shedding behind square cylinder using splitter plate." *Engineering Applications of Computational Fluid Mechanics* 2, no. 4 (2008): 514-524.
[9] Silva-Ortega, M., and Gustavo Roque da Silva Assi. "Suppression of the vortex-induced vibration of a circular cylinder surrounded by eight rotating wake-control cylinders." *Journal of Fluids and Structures* 74 (2017): 401-412.
[10] Xu, Feng, Wen-Li Chen, Wei-Feng Bai, Yi-Qing Xiao, and Jin-Ping Ou. "Flow control of the wake vortex street of a circular cylinder by using a traveling wave wall at low Reynolds number." *Computers & Fluids* 145 (2017): 52-67.
[11] Canpolat, Cetin. "Characteristics of flow past a circular cylinder with a rectangular groove." *Flow Measurement and Instrumentation* 45 (2015): 233-246.

[12] Zhou, Bo, Xikun Wang, Wei Guo, Jiaxin Zheng, and Soon Keat Tan. "Experimental measurements of the drag force and the near-wake flow patterns of a longitudinally grooved cylinder." *Journal of Wind Engineering and Industrial Aerodynamics* 145 (2015): 30-41.
[13] Akilli, Huseyin, Besir Sahin, and N. Filiz Tumen. "Suppression of vortex shedding of circular cylinder in shallow water by a splitter plate." *Flow Measurement and Instrumentation* 16, no. 4 (2005): 211-219.
[14] Bao, Yan, and Jianjun Tao. "The passive control of wake flow behind a circular cylinder by parallel dual plates." *Journal of Fluids and Structures* 37 (2013): 201-219.
[15] Soumya, S., and K. Arul Prakash. "Effect of splitter plate on passive control and drag reduction for fluid flow past an elliptic cylinder." *Ocean Engineering* 141 (2017): 351-374.
[16] Liu, Kai, Jianqiang Deng, and Mei Mei. "Experimental study on the confined flow over a circular cylinder with a splitter plate." *Flow Measurement and Instrumentation* 51 (2016): 95-104.
[17] Ozkan, Gokturk M., Erhan Firat, and Huseyin Akilli. "Passive flow control in the near wake of a circular cylinder using attached permeable and inclined short plates." *Ocean Engineering* 134 (2017): 35-49.
[18] Franke, R., W. Rodi, and B. Schönung. "Numerical calculation of laminar vortex-shedding flow past cylinders." *Journal of Wind Engineering and Industrial Aerodynamics* 35 (1990): 237-257.
[19] Moukalled, Fadl, L. Mangani, and Marwan Darwish. *The finite volume method in computational fluid dynamics*. Vol. 113. Berlin, Germany:: Springer, 2016.
[20] Qu, Lixia, Christoffer Norberg, Lars Davidson, Shia-Hui Peng, and Fujun Wang. "Quantitative numerical analysis of flow past a circular cylinder at Reynolds number between 50 and 200." *Journal of Fluids and Structures* 39 (2013): 347-370.
[21] Park, Jeongyoung, Kiyoung Kwon, and Haecheon Choi. "Numerical solutions of flow past a circular cylinder at Reynolds numbers up to 160." *KSME international Journal* 12, no. 6 (1998): 1200-1205.
[22] Tawekal, Jessica Rikanti. "CFD simulation of the Flow over a 2-Dimensional Pipe and Vortex Induced Vibration of the Pipe with 1 Degree of Freedom." Master's thesis, University of Stavanger, Norway, 2015.
[23] Braza, M., P. H. H. M. Chassaing, and H. Ha Minh. "Numerical study and physical analysis of the pressure and velocity fields in the near wake of a circular cylinder." *Journal of fluid mechanics* 165 (1986): 79-130.
[24] Tritton, David J. "Experiments on the flow past a circular cylinder at low Reynolds numbers." *Journal of Fluid Mechanics* 6, no. 4 (1959): 547-567.
[25] Nieuwstadt, F., and H. B. Keller. "Viscous flow past circular cylinders." *Computers & Fluids* 1, no. 1 (1973): 59-71.
[26] Behr, M., D. Hastreiter, S. Mittal, and T. E. Tezduyar. "Incompressible flow past a circular cylinder: dependence of the computed flow field on the location of the lateral boundaries." *Computer Methods in Applied Mechanics and Engineering* 123, no. 1-4 (1995): 309-316.
[27] Mittal, Sanjay, and Saurav Singh. "Vortex-induced vibrations at subcritical Re." *Journal of Fluid Mechanics* 534 (2005): 185-194.
[28] Singha, Sintu, and K. P. Sinhamahapatra. "Flow past a circular cylinder between parallel walls at low Reynolds numbers." *Ocean Engineering* 37, no. 8-9 (2010): 757-769.
[29] Li, Yanbing, R. Zhang, R. Shock, and H. Chen. "Prediction of vortex shedding from a circular cylinder using a volumetric Lattice-Boltzmann boundary approach." *The European Physical Journal Special Topics* 171, no. 1 (2009): 91-97.
[30] Hwang, Jong-Yeon, Kyung-Soo Yang, and Seung-Han Sun. "Reduction of flow-induced forces on a circular cylinder using a detached splitter plate." *Physics of Fluids* 15, no. 8 (2003): 2433-2436.